JACS
JOURNAL OF THE AMERICAN CHEMICAL SOCIETY

Article

pubs.acs.org/JACS

Extended π-Conjugated System for Fast-Charge and -Discharge Sodium-Ion Batteries

Chengliang Wang,[†] Yang Xu,[†] Yaoguo Fang,[†] Min Zhou,[†] Liying Liang,[†] Sukhdeep Singh,[‡] Huaping Zhao,[†] Andreas Schober,[‡] and Yong Lei*[,†]

[†]Institute for Physics and IMN MacroNano and [‡]Institute for Chemistry and Bio-Technique and IMN MacroNano, Technical University of Ilmenau, Ilmenau 98693, Germany

Supporting Information

ABSTRACT: Organic sodium-ion batteries (SIBs) are potential alternatives of current commercial inorganic lithium-ion batteries for portable electronics (especially wearable electronics) because of their low cost and flexibility, making them possible to meet the future flexible and large-scale requirements. However, only a few organic SIBs have been reported so far, and most of them either were tested in a very slow rate or suffered significant performance degradation when cycled under high rate. Here, we are focusing on the molecular design for improving the battery performance and addressing the current challenge of fast-charge and -discharge. Through reasonable molecular design strategy, we demonstrate that the extension of the π-conjugated system is an efficient way to improve the high rate performance, leading to much enhanced capacity and cyclability with full recovery even after cycled under current density as high as 10 A g^{-1}.

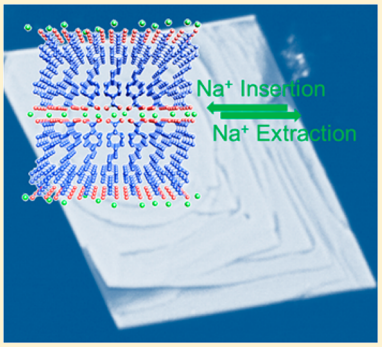

INTRODUCTION

Rechargeable lithium-ion batteries have played an important role in power supply for portable electronic devices in the past two decades.[1−7] However, it meets a fatal challenge that the resources of lithium will run out in a few years. Researchers have found that rechargeable sodium-ion batteries (SIBs) are one of the most promising alternative candidates for the next-generation battery systems, based on much cheaper, nontoxic, and more abundant sodium-based materials. The reason is that sodium-based materials have similar electrochemical process with lithium-based materials and the electrochemical potential of sodium is similar to that of lithium (only 0.3 V more positive).[7−21] However, one challenge that the widely studied inorganic SIBs encounter is that the Na-ion is larger than Li-ion (diameter: 2.32 vs 1.80 Å), which may increase the difficulty of insertion/extraction of the Na-ions and even destroy the rigid structure of the materials. Besides, inorganic materials are limited resources and are always nondegradable. They usually need tedious synthesis and purification. Therefore, from a practical point of view, organic materials are more attractive alternatives for power supply especially in the future flexible and large-scale applications. This is due to the various advantages of organic materials: lightweight, flexibility, vast resources, solution processability, recyclability, and easily functionalized for improving the electrochemical performance.[1−4,12−31] However, until now, only a few organic materials have been applied in SIBs.[12−21] Even worse, most of the previously reported organic SIBs were tested in a very slow charge/discharge process (e.g., 10 mA g^{-1}, which takes a very long time for a charge/discharge cycle),[13−18] and those tested under fast charge/discharge process often led to significant performance degradation.[19−21] These naturally limit their potential applications.

In order to achieve high rate performance, there is no doubt that three aspects are very critical, including the charge transport and collection, the stability of the charged and discharged states, and the ion diffusion. Inspired from the molecular design of organic semiconductors in organic electronics where the extended π-conjugated system can not only stabilize the +1 or −1 charged states but also facilitate the charge transport,[31] we herein focus on the molecular design, i.e., using the advantages of extended π-conjugated system for improving the battery performance and addressing the current challenge of fast-charge and -discharge. The extension of the π-conjugated system is predictable to be conducive to fast charge transport and collection and to improve the toleration to the fast insertion/extraction of Na-ions during the fast-charge and -discharge process. Simultaneously, extending the π-conjugated system is also helpful to strengthen the intermolecular interactions (e.g., π−π or C−H···π interactions) which might lead to a layer-by-layer molecular arrangement. This layer-by-layer molecular arrangement is expected to form a fast route for ion diffusion between two layers. In order to verify our assumption, the first and widely reported small molecule[29] for organic sodium batteries, sodium benzene-dicarboxylate (SBDC, Figure 1a),[17−19] is selected as starting molecule. In order to extend its π-conjugated system, three possible linkages, including carbon−carbon single, double, and triple bond, can be used to form extended π-conjugated molecules, giving

Received: January 12, 2015
Published: February 9, 2015

DOI: 10.1021/jacs.5b00336
J. Am. Chem. Soc. 2015, 137, 3124−3130

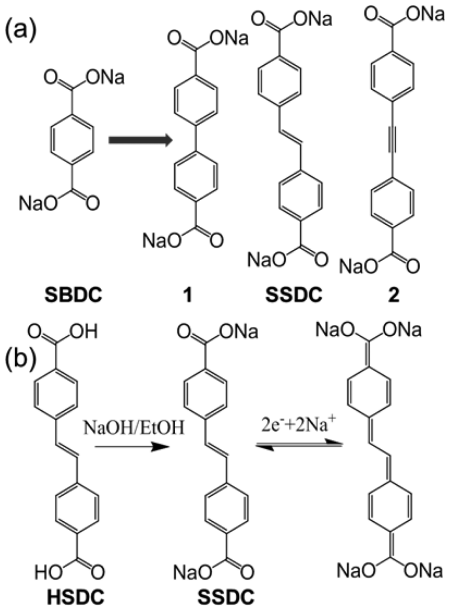

Figure 1. (a) Schematic chemical structure of starting molecule SBDC and three possible linkages to extend its π-conjugation, forming 1, SSDC, and 2 respectively. (b) Schematic diagram for the synthesis and reversible Na-ion insertion/extraction mechanism of SSDC.

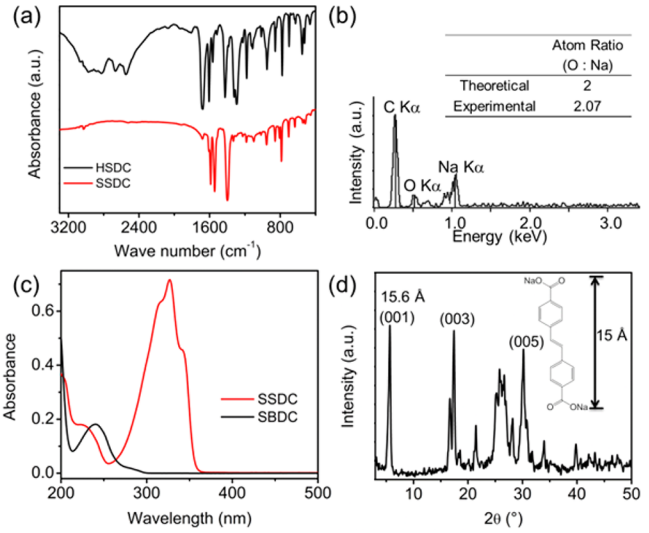

Figure 2. (a) FTIR spectra of SSDC and its reactant HSDC. (b) EDS spectra of SSDC. Inset of (b), the theoretical and experimental atom ratio of oxygen and sodium. (c) UV–vis absorption spectra of SSDC and SBDC in water solution. (d) XRD patterns of SSDC powder, inset of (d) shows the chemical structure and the roughly calculated molecular length of SSDC.

molecule 1, SSDC (sodium 4,4′-stilbene-dicarboxylate), and 2 respectively (Figure 1a). The literatures have shown that the C–C single bond would lead to a nonplanar structure because of the steric hindrance between the adjacent aromatic rings,[16,31–33] which unambiguously harms the extension of π-conjugation and thus impairs the charge transport and electric stability.[34–36] Similarly, due to its electron cloud shape and the possible rotation (also leading to nonplanar structure), the C≡C bond linked material possesses a lower π-conjugation than that of C=C bond based material as well.[31,36,37] Therefore, here, the carbon–carbon double bond is selected as the linkage to extend the π-conjugated system of SBDC. Considering the further increase in the molecular weight will decrease the specific capacity, SSDC, containing two benzene rings and offering a theoretical specific capacity of 172 mAh g^{-1}, is designed as a model to investigate the influence of extended π-conjugated system on the fast-charge and -discharge sodium batteries.

The present report shows that the reasonable molecular design indeed efficiently increases the π-conjugation of the material. This leads to an improved reversible capacity of 220 mAh g^{-1} under the current density of 50 mA g^{-1}, although the nearly doubled molecular weight should largely decrease its theoretical specific capacity. Remarkably, the reasonable extension of the π-conjugation delivered much better high rate performance than the starting molecule and can be fully recovered even after cycled at rate as high as 10 A g^{-1}. This performance is among the highest performances for organic SIBs.

RESULTS AND DISCUSSION

The synthesis and the corresponding redox reaction of SSDC are presented in Figure 1b. SSDC was synthesized for the first time through an environmentally friendly one-pot reaction of 4,4-stilbenedicarboxylic acid (HSDC) with sodium hydroxide in ethanol according to a literature procedure[29] (for details see Experimental section). From the FT-IR spectra (Figure 2a), it is clear that the broad peak in the range from 3000 to 2500 cm^{-1} which belongs to the stretching vibration of O–H bond disappeared in the spectrum of the product SSDC. On the other hand, the fingerprint peaks of carboxylic acid around 1680 cm^{-1} which is identified to the stretching vibration of C=O bond and around 1320 and 1290 cm^{-1} which can be assigned to the stretching vibration of C–O bond also disappeared. These results indicate the pure formation of SSDC. The ^{1}H NMR and ^{13}C NMR (300 MHz, D_2O) further confirmed the formation and purity of the sodium carboxylates (see Figures S1 and S2).The energy dispersive spectroscopy (EDS) spectra (Figure 2b) showed the existence of sodium, with an atom ratio of oxygen and sodium (2.07:1) equal to the theoretical ratio (2:1). All of these confirmed the formation and purity of our model molecule. Figure 2c shows the UV–vis absorption spectra of SSDC and SBDC in water solution at the concentration of 10^{-5} M. Clearly, the maximum absorption of SSDC was red shifted by more than 50 nm compared with SBDC, indicating a much smaller HOMO–LUMO (highest occupied molecular orbit and lowest unoccupied molecular orbit) energy gap of SSDC (3.49 and 4.18 eV for SSDC and SBDC, respectively). The smaller energy gap of SSDC implies a much larger π-conjugated system through our efficient molecular design and thereby a higher electric stability and conductivity.[27,37]

The self-assembly characteristics of SSDC is conducted by using drop-casting of SSDC solution in water onto silicon substrates, which resulted in two-dimensional (2D) micrometer sized plates with mica-like terrace surface, as shown Figure 3a. This mica-like terrace edges can also be observed in the as-prepared submicrometer-sized product of SSDC from the one-pot reaction (see scanning electron microscopy (SEM) images in Figures S3 and S4). On the other hand, the self-assembly of SBDC showed microrod morphologies (Figure 3b). According to the Bravais–Friedel–Donnay–Harker (BFDH) rules,[31,35,38,39] the crystals are preferable to grow along the direction with strong intermolecular interactions. Therefore, this terrace morphology suggests that the intermolecular

DOI: 10.1021/jacs.5b00336
J. Am. Chem. Soc. 2015, 137, 3124–3130

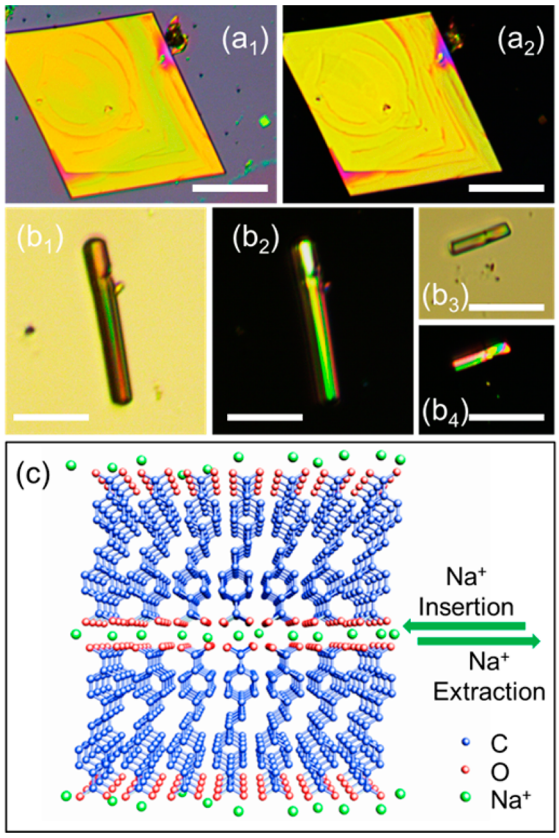

Figure 3. (a_1) Photo image and (a_2) corresponding cross-polarized light microscopy (PLM) image of a typical SSDC crystal. (b_1, b_3) Photo images and (b_2, b_4) their corresponding PLM images of typical SBDC crystals. The uniform brightness of PLM images of SSDC and SBDC suggest that the self-assembly crystals are single crystalline. Scale bar: 30 μm. (c) Schematic molecular packing of SSDC: the molecules are stacking layer-by-layer with strong $\pi-\pi$ intermolecular interaction in plane and carboxylate group situated on the surface of the layers, forming a channel exactly at the active center for insertion/extraction of Na-ions between layers.

interactions of SSDC along the short axis ($\pi-\pi$ or C−H···π interactions) are much stronger than that of the long axis direction where only weak van der Waals' force exists. This implies that the extension of the π-conjugated system enhanced the intermolecular interactions of SSDC, and the SSDC molecules are packing as layer-by-layer mode (Figure 3c). The X-ray diffraction (XRD) pattern further proves this assumption (Figure 2d). From the XRD pattern, the product exhibited strong (00*l*) peaks. The *d*-spacing of (00*l*) is around 15.6 Å, which is close to the calculated molecular length (14−15 Å, by roughly using the carbon−carbon bond length of 1.4 Å, the length of C═O bond of 1.2 Å and the diameter of Na-ion of 2.32 Å). According to the Crystallography Open Database (COD number: 7105617), the molecular length of the carboxylate anion (SDC^{2-}) is also around 14 Å, giving a total molecular length of about 14.5 Å. The atomic force microscopy (AFM) image of the crystal surface shows that the typical step height of the terrace layers was about 3.2 nm, almost equal to two times of the molecular length (Figure S5). The agreement between the experimental length and the theoretical value suggests that the molecules adopt a lamellar packing motif with the carboxylate groups situated on the two surfaces of each layer in the solid states (Figure 3c). Such kind of packing and the larger *d*-spacing distance than the length of molecules make it possible to form a fast diffusion channel for insertion/extraction of Na-ions into/from the interspace between the layers, where the electrochemical reaction happens.

To verify our assumption that the extended π-conjugation is really beneficial to the battery performance, the electrochemical performance of SSDC electrode was investigated by using a half cell with a sodium metal as the counter electrode. The SSDC electrodes were obtained by mixing the products with carbon black (Super-P) as conductive additive and sodium carboxymethyl cellulose (CMC) as binder in water. Figure 4a shows

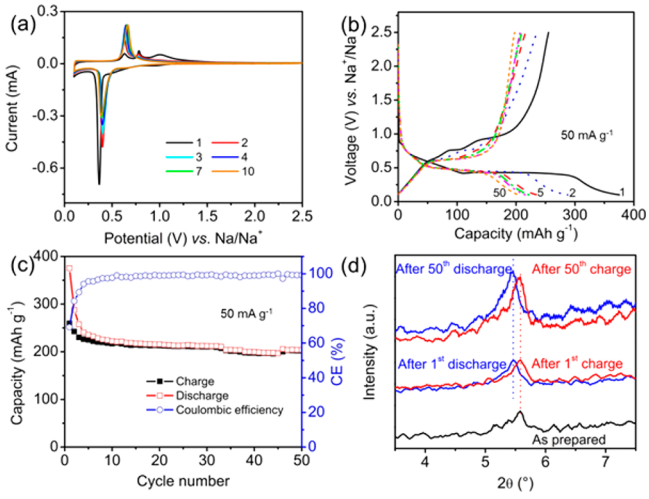

Figure 4. (a) Typical CV curves of SSDC films in the first 10 cycles; (b and c) Electrochemical performances of SSDC: (b) Voltage profiles (1st, 2nd, 5th, 10th, 20th, and 50th cycles are selected as representatives) and (c) cyclability. (d) XRD patterns of as-prepared SSDC films and XRD patterns of SSDC films after discharging to 0.1 V (vs Na/Na^+) and after charging to 2.5 V (vs Na/Na^+).

typical cyclic voltammograms (CV) of the half-cell. From the CV curves, SSDC showed one reduction peak around 0.39 V (vs Na/Na^+) during the cathodic scan, corresponding to the insertion of two Na-ions. This potential is higher than that of SBDC (0.18 V, Figure S6), indicating that the extended π-conjugated system can significantly increase the redox potential. The anodic scan gives an oxidization peak around 0.66 V (vs. Na/Na^+), which suggests the extraction of Na-ions. The currents of the reduction peaks decrease gradually in the first seven cycles and become steady afterward. On the other hand, the curves of the anodic scan do not change obviously after the second cycle. Moreover, the intensity of the reduction peaks becomes similar to that of the oxidization peaks after seven cycles. These suggest an irreversible reduction of the electrolyte in the first seven cycles, which probably can be ascribed to the irreversible formation of solid electrolyte interphase (SEI). The currents of the reduction and oxidization become matched with each other after seven cycles, indicating that the redox reaction is reversible. The stability of the current after seven cycles also suggests that the former irreversible reduction should be due to the SEI phenomenon and the reversible electrochemical reaction is originated from the active material SSDC. Because the oxidization peak of monosodium product should be at a lower electric potential,[16] the peaks around 0.78 and 1.0 V which disappear in the subsequent cycles are probably originated from the additive, trace amorphous SSDC or ion adsorption (also see below).

DOI: 10.1021/jacs.5b00336
J. Am. Chem. Soc. 2015, 137, 3124−3130

Figure 4b shows the charge−discharge profiles of the SSDC electrodes between 2.5 and 0.1 V at a rate of 50 mA g^{-1}. The first discharge delivers a capacity of about 375 mAh g^{-1}. However, upon the recharge, a capacity of about 260 mAh g^{-1} was observed, giving a low Coulombic efficiency (CE) of the first cycle (ca. 69%). This probably could be ascribed to the irreversible SEI phenomenon, trace amorphous SSDC or ion adsorption, which can be inferred from the difference of discharge profiles between first and subsequent cycles within the voltage range from 0.7 to 0.4 V. From the 10th cycle, the Coulombic efficiency becomes higher than 98% (Figure 4c). There are three clear plateaus located at ca. 0.95, 0.75, and 0.61 V in the first recharge profile. The plateau at ca. 0.95 V, which also can be observed in the CV curve (~1.0 V in Figure 4a), could be attributed to the ion adsorption rather than resistance interface, which will disappear in the subsequent cycles (see Figure S7).[40] The plateau at 0.75 V (~0.78 V in Figure 4a) can be assigned to the contribution of Super-P (Figure S8), which is much smaller than SSDC and thereby is covered by the plateau of SSDC during cycling (Figure 4a,b). The plateau at 0.61 V (~0.66 V in Figure 4a), corresponding to the plateau at 0.45 V in the discharge profile, can be ascribed to the reversible oxidization/reduction of the two carbonyl groups with extraction/insertion of two Na cations. Because of the safety problem[17,41] from the formation of the Na metal dendrite arisen around 0 V and the potential irreversible reaction of the mixed carbon materials and electrolyte (Figure S8), the redox potential of SSDC is ideal as anode material for SIBs. As a control experiment, this plateau is about 0.2 V higher than that of the SBDC electrodes (see Figure S6). In addition, the capacity becomes stable after the 10th cycle, giving a capacity as high as 222 mAh g^{-1} and keeping 204 mAh g^{-1} after 50 cycles with a capacity retention higher than 90% (Figure 4c), suggesting its excellent cyclability. Considering the weight ratio of the active material and carbon black, the total theoretical capacity should be the sum capacity of the active material and the carbon black, which equals to 252 mAh g^{-1} (=172 + 100 mAh g^{-1} × 40 wt % Super P/50 wt % SSDC) with at most 80 mAh g^{-1} contributed from carbon black. Therefore, the obtained value is almost close to the theoretical capacity. This capacity is among the highest values for both organic lithium and sodium batteries. On the other hand, under the same condition, the SBDC (which has a much smaller π-conjugated system) electrodes only deliver a capacity of 192 mAh g^{-1} for the second cycle and decrease to 162 mAh g^{-1} after 50 cycles (Figure S6), although the molecular weight of SSDC is nearly doubled of SBDC (total theoretical capacity of SBDC electrodes: 335 mAh g^{-1} (=255 + 100 mAh g^{-1} × 40 wt % Super P/50 wt % SBDC) leading to a much smaller theoretical specific capacity. These results prove that the appropriate extension of the π-conjugated system can increase the capacity and improve the cyclability.

In order to investigate the influence of extended π-conjugated system on fast-charge and -discharge processes, the SSDC and SBDC electrodes are tested under different high rates. The high rate performance are important properties for the practical application. Remarkably, the SSDC electrodes exhibited much better rate performance than SBDC (Figure 5a). It delivers a capacity higher than 100 mAh g^{-1} even at a 2 A g^{-1} rate. The capacities at 5 A g^{-1} and 10 A g^{-1} are still as high as 90 and 72 mAh g^{-1}, respectively. In this case, only several minutes or even tens of seconds are required for a full charge. The capacity also can be fully recovered after cycled at

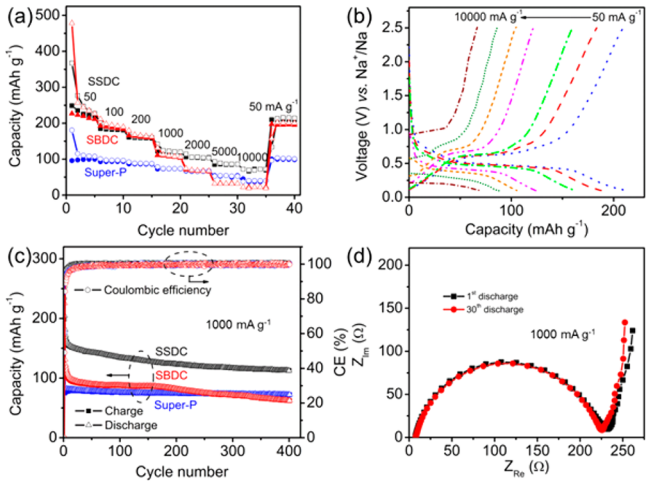

Figure 5. Electrochemical performances of SSDC: (a) rate cyclability (black squares, the rate cyclability of Super-P (blue circles) and SBDC (red triangles) are also presented for comparison), solid symbols: charge, open symbols: discharge; and (b) rate capability (right to left: from 50, 100, 200 mA g^{-1} to 1, 2, 5, and 10 A g^{-1}). (c) Cyclability of SSDC (black, the rate capability of Super-P (blue) and SBDC (red) are also presented for comparison) under current density of 1 A g^{-1} and (d) Nyquist plots of SSDC after discharging to 0.1 V under current density of 1 A g^{-1} in the frequency range from 1 MHz to 5 mHz.

rate as high as 10 A g^{-1} (Figure 5a). From Figure 5b, it is clear that the plateau for reduction/oxidization of SSDC in the discharge/charge profiles only change slightly (~0.1 V) at 5 A g^{-1}. The plateau of SSDC still exists at 10 A g^{-1} with reduction potential around 0.25 V (a 0.2 V shift). This is meaningful, because as mentioned above a suitable redox potential is very important to prevent the possible formation of Na metal dendrite and other degradation around 0 V. However, as a control experiment, the discharge profile of SBDC becomes sloping when the current density increases to 1 A g^{-1} and all the capacity of SBDC is distributed to potential lower than 0.2 V at 5 A g^{-1} (Figure S6, also see literature).[17] Similarly, all the capacity of Super-P is distributed to potential lower than 0.1 V at 10 A g^{-1} (Figure S8). From Figure 5a, it is clear that in our condition, the SSDC electrodes deliver a capacity a little higher than that of SBDC when charged/discharged slowly, although its theoretical capacity is lower (also see Figure 4b-c and S6). However, under fast-charge and −discharge rate, SSDC showed a much better rate performance than that of SBDC. The capacity of SBDC degraded to 32 and 22 mAh g^{-1} at 5 A g^{-1} and 10 A g^{-1}, respectively. These values are even lower than those of Super-P (54 and 40 mAh g^{-1} at 5 A g^{-1} and 10 A g^{-1}, respectively), which may be due to an increasing resistance interface of SBDC during cycling (see following).

Figure 5c shows the cyclability of the SSDC electrodes at a 1 A g^{-1} rate, delivering a capacity of 247 mAh g^{-1} for the first cycle with Coulombic efficiency as high as 80%. Incredibly, the Coulombic efficiency increases to 98% after 5 cycles, giving a capacity up to 160 mAh g^{-1}. After 400 cycles, the capacity is still as high as 112 mAh g^{-1} with retention higher than 70%. Figure 5c shows a visible comparison of SSDC and SBDC electrodes measured under current density of 1 A g^{-1}, in which SBDC also provides a comparable capacity of 225 mAh g^{-1} for the first cycle but with Coulombic efficiency as low as 49%. The capacity kept on decreasing to 95 mAh g^{-1} in the first 20 cycles with Coulombic efficiency lower than 98%. After 150 cycles, its

DOI: 10.1021/jacs.5b00336
J. Am. Chem. Soc. 2015, 137, 3124−3130

capacity deceases dramatically leading to a capacity even lower than individual Super-P. Its capacity degraded to 62 mAh g^{-1} after 400 cycles. These results show that the extension of π-conjugated system is also capable to improve the capacity and cyclability under fast-charge and -discharge rates.

In order to get a further insight of the SSDC electrodes during the cycling, the ex situ measurement of its SEM images, EDS spectra, XRD patterns, and electrochemical impedance spectra (EIS) are studied. From the SEM images of the SSDC electrodes (Figure S3), it is clear that even after 50 cycles of discharge and charge cycles, the morphology change is negligible. All of them exhibit terrace morphology. The diffraction peak of the films (Figure 4d) after first discharge shows a slight shift from 15.8 to16.1 Å. The [001] *d*-spacing of the thin films (15.8 Å) is a little larger than that of the powders (15.6 Å, Figure 2d), which is probably due to the different solvents (ethanol for the powders and water for the thin films). On the other hand, this [001] *d*-spacing exhibited a slight increase after discharge (from 15.8 to16.1 Å), which is understandable because both of the insertion of the Na-ions and the decreased unsaturation bonds in the discharged state will elongate the molecule. This is also the reason that only variation of the [001] *d*-spacing is presented here because the strongest diffraction and the largest variation exist in the *c* axis. However, the volume change even along this axis is negligible (from 15.8 to16.1 Å, < 2%), which can be ascribed to the softness of the organic materials and the weaker intermolecular interactions between two layers (this also confirmed the assumption that the strong $\pi-\pi$ intermolecular interaction facilitates a lamellar stacking). The *d*-spacing can be recovered after recharge and did not show any obvious change even after charge and discharge 50 cycles. The absence of a phase transformation,[42] the slight variation of *d*-spacing after discharge, the recovery of the *d*-spacing after charge, and the terrace structure suggest there is a preferential route between two layers for diffusion of Na-ions (Figure 3c), which probably is one reason that the electrodes can give high performance even charged/discharged under high current densities. EDS spectra are used for analyzing the change of the elemental components in the electrodes during cycling. Because CMC also contains oxygen, poly(vinylidenedifluoride) (PVDF) instead of CMC was utilized as the binder in these electrode films. On the other hand, CMC is chosen as the binder in the battery test because of it's higher conductivity, environmentally friendly (the solvent is water), and low cost.[17,40] Furthermore, the active material is soluble in water but insoluble in NMP (the solvent for PVDF), which results in a better mixing than that of PVDF. This will improve the charge transport and the diffusion of the electrolyte. The EDS spectra of the films show a clear variation of oxygen and Na-atom ratio from 2.07, 1.08 to 1.70, which agrees well with the theoretical ratio from 2, 1 to 2 (Figure S9 and Table S1). This result reconfirmed the mechanism that the insertion and extraction of the Na-ions are through the reduction and the subsequent oxidization of the C═O bonds, and there are no other side-reactions or additional mechanisms to contribute the total electrochemical performance.[17−19,28,29] The ratio after recharge is a little lower than the theoretical ratio, which can be ascribed to the lower stability (Figures S4 and S10) and worse compatibility of PVDF binder (PVDF is a lyophobic material, which is not good for the diffusion of electrolyte). The EIS measurements were carried out in the frequency range from 1 MHz to 5 mHz for investigating the Na-ions diffusion in the electrolyte and migration through the SEI and the charge transfer through the SEI and diffusion in the electrodes. Figure 5d shows the Nyquist plots of SSDC electrodes after discharging to 0.1 V during cycling. Interestingly, the impedance shows insignificant change even after 30 charge/discharge cycles with resistance around 108 Ω, suggesting the stability of the electrodes during cycling. On the other hand, the impedance especially the semicircle in the middle-frequency region increases dramatically during the cycling in the Nyquist plots of the SBDC electrodes, indicating that the interface resistance increases during cycling, which may be a reason that the SBDC electrode showed much worse performance (Figure S11). This increase of the interface resistance might be ascribed to the short π-conjugated system of SBDC, which leads to lower charge transport and stability. From these analyses, we believed that the high capacities with high cyclability of SSDC electrodes are probably due to the extended π-conjugated system because it can: (1) improve the charge transport and stabilize the charged and discharged states and (2) enhance the intermolecular interactions and the resulted terrace packing structure facilitates the insertion/extraction of the Na-ions. It should be noted that SSDC also showed a much better high rate performance than that of the material[16] with carbon−carbon single bond linkage, which again proved the efficiency of extending π-conjugated system on high rate performance.

■ CONCLUSIONS

In summary, we reasonably designed SSDC for SIBs, through the molecular design to appropriately extend the π-conjugated system for improving the battery performance and addressing the current challenge of fast-charge and -discharge. As expected, the extension of the π-conjugated system was proved to be an efficient method for improving the electrochemical performance, delivering a reversible capacity of 220 mAh g^{-1} under current density of 50 mA g^{-1}. This capacity is among the highest values for both organic Li- and Na-ion batteries. Remarkably, the designed electrodes showed much enhanced high rate performance with reversible capacities of 105 mAh g^{-1} at current density of 2 A g^{-1} and 72 mAh g^{-1} at current density as high as 10 A g^{-1}, which is much better than the starting molecule and superior in organic SIBs. The capacity also can be fully recovered even after cycled at rate as high as 10 A g^{-1}. The cyclability performance under high current density of 1 A g^{-1} showed that the capacity is still higher than 112 mAh g^{-1} even after 400 cycles with retention higher than 70%. These results suggest that the extension of π-conjugated system is an efficient strategy to improve the high rate performance, probably because it can: (1) improve the charge transport and stabilize the charged and discharged states and (2) enhance the intermolecular interactions and the resulted terrace packing structure can facilitate the insertion/extraction of the Na-ions. We believe this work will arouse growing interests of organic materials for SIBs with functional molecular design toward high performance and pave a way to achieve flexible application of SIBs in large-scale portable and wearable electronics.

■ EXPERIMENTAL SECTION

Synthesis of SSDC. Sodium 4,4′-stilbene-dicarboxylate was prepared according to the literature reported for lithium terephthalate preparation.[29] 4,4′-Stilbenedicarboxylic acid (1.00 g, 3.73 mmol) and sodium hydroxide (0.31 g, 7.83 mmol) were added into 30 mL EtOH at room temperature. After stirring overnight, the suspended mixture was filtrated. The product was washed with EtOH three times,

DOI: 10.1021/jacs.5b00336
J. Am. Chem. Soc. 2015, 137, 3124−3130

accompanied with supersonic for better dissolution of the impurities. This procedure led to a white solid of 1.15 g (yield: 99%). The product was dried in vacuum at 110 °C for overnight. Compounds, reagents, and solvents were purchased and used directly without further purification.

Characterization. The SEM images and EDS spectra were taken by using a Hitachi S4800 instrument employing voltages of 5 and 10 kV, respectively. AFM images were carried out on a NT-MDT instrument. IR spectra were performed on a Tensor-27 from Bruker. UV−vis absorption spectra were measured by a UV−vis spectrophotometer (SP 3000 plus). NMR spectra were recorded on a Varian 300 MHz spectrometer in D_2O. The XRD measurements were recorded on a Bruker-axs Discover D8 applying Cu Kα (1.54056 Å) radiation equipment. The CVs and electrochemical impedance spectroscopy were conducted on a BioLogic VSP potentiostat. The CVs were scanned in the potential range from 0.1 to 2.5 V at a scan rate of 0.1 mV s^{-1}. The ex situ measurements are accomplished by immediately disassembling the batteries after charging/discharging and washing by propylene carbonate (PC) in N_2-filled glovebox.

Electrochemical Characterization. Samples of electrochemically active materials (SSDC or SBDC) were mixed with carbon black (Super P) and CMC at a weight ratio of 50:40:10 and then coated uniformly using a doctor-blade on a copper foil with roughly 1 mg cm^{-2} mass loading. The solvent is water. The Super P films mixed with CMC at a weight ratio of 40:10 were obtained by using same method. The samples for EDS spectra were mixed with PVDF in *N*-methyl-2-pyrrolidone (NMP). The electrodes were dried at 110 °C under vacuum overnight. The electrochemical performance was evaluated by using 2032 coin cells with a Na metal anode and 1.0 M $NaClO_4$ in PC electrolyte solution. The half-cell batteries were assembled in a N_2-filled glovebox. Sodium metal was used as a counter electrode, and the two electrodes were separated by a glass fiber separator (Whatman, GF/B). Galvanostatic experiments were performed at a different current densities at a potential range of 2.5−0.1 V (vs Na/Na^+) using a LANHE-CT2001A test system (Wuhan, China) under room temperature.

■ ASSOCIATED CONTENT

Supporting Information

^1H NMR and ^{13}C NMR spectra, AFM and SEM images, and EDS spectra of SSDC electrodes, electrochemical performance of Super-P and SBDC, and Nyquist plots of SSDC and SBDC electrodes. This material is available free of charge via the Internet at http://pubs.acs.org.

■ AUTHOR INFORMATION

Corresponding Author

*yong.lei@tu-ilmenau.de

Notes

The authors declare no competing financial interest.

■ ACKNOWLEDGMENTS

The authors acknowledge the financial support from European Research Council (ThreeDsurface: 240144), BMBF (ZIK-3DNanoDevice: 03Z1MN11), BMBF (Meta-ZIK-BioLitho-Morphie: 03Z1M511), Volkswagen-Stiftung (Herstel-lung funktionaler Oberflächen: I/83 984,) and National Natural Science Foundation of China (51203067). The authors also thank the help from Dr. Qing Meng, Dr. Xiaotao Zhang and Mr. Wenxin Wang for IR, NMR, and AFM measurements. The authors also appreciate the technical support from Dr. Henry Romanus, Dr. Arne Albrecht, and Ms. Moumou Li.

■ REFERENCES

(1) Liang, Y.; Tao, Z.; Chen, J. *Adv. Energy Mater.* **2012**, *2*, 742−769.
(2) Inatomi, Y.; Hojo, N.; Yamamoto, T.; Watanabe, S.-i.; Misaki, Y. *ChemPlusChem.* **2012**, *77*, 973−976.
(3) Nokami, T.; Matsuo, T.; Inatomi, Y.; Hojo, N.; Tsukagoshi, T.; Yoshizawa, H.; Shimizu, A.; Kuramoto, H.; Komae, K.; Tsuyama, H.; Yoshida, J.-i. *J. Am. Chem. Soc.* **2012**, *134*, 19694−19700.
(4) Chen, H.; Armand, M.; Courty, M.; Jiang, M.; Grey, C. P.; Dolhem, F.; Tarascon, J.-M.; Poizot, P. *J. Am. Chem. Soc.* **2009**, *131*, 8984−8988.
(5) Armand, M.; Tarascon, J. M. *Nature* **2008**, *451*, 652−657.
(6) Zhou, G.; Li, F.; Cheng, H.-M. *Energy Environ. Sci.* **2014**, *7*, 1307−1338.
(7) Kim, S.-W.; Seo, D.-H.; Ma, X.; Ceder, G.; Kang, K. *Adv. Energy Mater.* **2012**, *2*, 710−721.
(8) Park, Y.-U.; Seo, D.-H.; Kwon, H.-S.; Kim, B.; Kim, J.; Kim, H.; Kim, I.; Yoo, H.-I.; Kang, K. *J. Am. Chem. Soc.* **2013**, *135*, 13870−13878.
(9) Hibino, M.; Harimoto, R.; Ogasawara, Y.; Kido, R.; Sugahara, A.; Kudo, T.; Tochigi, E.; Shibata, N.; Ikuhara, Y.; Mizuno, N. *J. Am. Chem. Soc.* **2013**, *136*, 488−494.
(10) Darwiche, A.; Marino, C.; Sougrati, M. T.; Fraisse, B.; Stievano, L.; Monconduit, L. *J. Am. Chem. Soc.* **2012**, *134*, 20805−20811.
(11) Palomares, V.; Casas-Cabanas, M.; Castillo-Martinez, E.; Han, M. H.; Rojo, T. *Energy Environ. Sci.* **2013**, *6*, 2312−2337.
(12) Deng, W.; Liang, X.; Wu, X.; Qian, J.; Cao, Y.; Ai, X.; Feng, J.; Yang, H. *Sci. Rep.* **2013**, *3*, 2671.
(13) Yao, M.; Kuratani, K.; Kojima, T.; Takeichi, N.; Senoh, H.; Kiyobayashi, T. *Sci. Rep.* **2014**, *4*, 3650.
(14) Castillo-Martínez, E.; Carretero-González, J.; Armand, M. *Angew. Chem., Int. Ed.* **2014**, *53*, 5341−5345.
(15) Luo, W.; Allen, M.; Raju, V.; Ji, X. *Adv. Energy Mater.* **2014**, *4*, 1400554.
(16) Choi, A.; Kim, Y. K.; Kim, T. K.; Kwon, M.-S.; Lee, K. T.; Moon, H. R. *J. Mater. Chem. A* **2014**, *2*, 14986−14993.
(17) Park, Y.; Shin, D.-S.; Woo, S. H.; Choi, N. S.; Shin, K. H.; Oh, S. M.; Lee, K. T.; Hong, S. Y. *Adv. Mater.* **2012**, *24*, 3562−3567.
(18) Abouimrane, A.; Weng, W.; Eltayeb, H.; Cui, Y.; Niklas, J.; Poluektov, O.; Amine, K. *Energy Environ. Sci.* **2012**, *5*, 9632−9638.
(19) Zhao, L.; Zhao, J.; Hu, Y.-S.; Li, H.; Zhou, Z.; Armand, M.; Chen, L. *Adv. Energy Mater.* **2012**, *2*, 962−965.
(20) Wang, S.; Wang, L.; Zhu, Z.; Hu, Z.; Zhao, Q.; Chen, J. *Angew. Chem., Int. Ed.* **2014**, *53*, 5892−5896.
(21) Sakaushi, K.; Hosono, E.; Nickerl, G.; Gemming, T.; Zhou, H.; Kaskel, S.; Eckert, J. *Nat. Commun.* **2013**, *4*, 1485.
(22) Song, Z.; Zhou, H. *Energy Environ. Sci.* **2013**, *6*, 2280−2301.
(23) Nishida, S.; Yamamoto, Y.; Takui, T.; Morita, Y. *ChemSusChem* **2013**, *6*, 794−797.
(24) Shin, J.-Y.; Yamada, T.; Yoshikawa, H.; Awaga, K.; Shinokubo, H. *Angew. Chem., Int. Ed.* **2014**, *53*, 3096−3101.
(25) Han, X.; Qing, G.; Sun, J.; Sun, T. *Angew. Chem., Int. Ed.* **2012**, *51*, 5147−5151.
(26) Huang, W.; Zhu, Z.; Wang, L.; Wang, S.; Li, H.; Tao, Z.; Shi, J.; Guan, L.; Chen, J. *Angew. Chem., Int. Ed.* **2013**, *52*, 9162−9166.
(27) Wang, S.; Wang, L.; Zhang, K.; Zhu, Z.; Tao, Z.; Chen, J. *Nano Lett.* **2013**, *13*, 4404−4409.
(28) Walker, W.; Grugeon, S.; Vezin, H.; Laruelle, S.; Armand, M.; Wudl, F.; Tarascon, J.-M. *J. Mater. Chem.* **2011**, *21*, 1615−1620.
(29) Armand, M.; Grugeon, S.; Vezin, H.; Laruelle, S.; Ribiere, P.; Poizot, P.; Tarascon, J. M. *Nat. Mater.* **2009**, *8*, 120−125.
(30) Nishide, H.; Oyaizu, K. *Science* **2008**, *319*, 737−738.
(31) Wang, C.; Dong, H.; Hu, W.; Liu, Y.; Zhu, D. *Chem. Rev.* **2012**, *112*, 2208−2267.
(32) Meng, H.; Sun, F. P.; Goldfinger, M. B.; Jaycox, G. D.; Li, Z. G.; Marshall, W. J.; Blackman, G. S. *J. Am. Chem. Soc.* **2005**, *127*, 2406−2407.
(33) Tripathi, A. K.; Heinrich, M.; Siegrist, T.; Pflaum, J. *Adv. Mater.* **2007**, *19*, 2097−2101.
(34) Zhang, X.; Yuan, G.; Li, Q.; Wang, B.; Zhang, X.; Zhang, R.; Chang, J. C.; Lee, C.-s.; Lee, S.-t. *Chem. Mater.* **2008**, *20*, 6945−6950.

DOI: 10.1021/jacs.5b00336
J. Am. Chem. Soc. 2015, 137, 3124−3130

(35) Wang, C.; Liu, Y.; Ji, Z.; Wang, E.; Li, R.; Jiang, H.; Tang, Q.; Li, H.; Hu, W. *Chem. Mater.* **2009**, *21*, 2840−2845.
(36) Wang, C.; Liu, Y.; Wei, Z.; Li, H.; Xu, W.; Hu, W. *Appl. Phys. Lett.* **2010**, *96*, 143302.
(37) Wang, C.; Wei, Z.; Meng, Q.; Zhao, H.; Xu, W.; Li, H.; Hu, W. *Org. Electron.* **2010**, *11*, 544−551.
(38) Donnay, J. D. H.; Harker, D. *Am. Mineral.* **1937**, *22*, 446−467.
(39) Wang, C.; Jiang, L.; Hu, W. *Organic/polymeric field-effect Transistors. In Organic Optoelectronics*, 1st ed.; Wiley-VCH: Weinheim, Germany, 2013; pp 95−170.
(40) Wang, Z.; Dupré, N.; Gaillot, A.-C.; Lestriez, B.; Martin, J.-F.; Daniel, L.; Patoux, S.; Guyomard, D. *Electrochim. Acta* **2012**, *62*, 77−83.
(41) Yu, H.; Ren, Y.; Xiao, D.; Guo, S.; Zhu, Y.; Qian, Y.; Gu, L.; Zhou, H. *Angew. Chem., Int. Ed.* **2014**, *53*, 8963−8969.
(42) Liu, H.; Strobridge, F. C.; Borkiewicz, O. J.; Wiaderek, K. M.; Chapman, K. W.; Chupas, P. J.; Grey, C. P. *Science* **2014**, *344*, 1252817.

DOI: 10.1021/jacs.5b00336
J. Am. Chem. Soc. 2015, 137, 3124−3130